ACADEMIC PRESS

Available online at www.sciencedirect.com
SCIENCE DIRECT®

Journal of Solid State Chemistry 170 (2003) 1–8

JOURNAL OF SOLID STATE CHEMISTRY

http://elsevier.com/locate/jssc

Synthesis and characterization of $La_4BaCu_5O_{13+\delta}$ and $La_4BaCu_{5-x}M_xO_{13+\delta}$: M = Fe, Co, Ni, Zn

P.S. Anderson,[a] C.A. Kirk,[a] J.M.S. Skakle,[b] and A.R. West[a]

[a] *Department of Engineering Materials, University of Sheffield, Sheffield S1 3JD, UK*
[b] *Department of Chemistry, University of Aberdeen, Aberdeen AB24 3UE, UK*

Abstract

$La_4BaCu_{5-x}M_xO_{13+\delta}$: M = Fe, Co, Ni, Zn were prepared by the solid-state route at 1000°C. Solid solution limits of $x = 1.0(1)$ [Fe], $x = 1.1(1)$ [Co], $x = 1.56(7)$ [Ni] and $x = 0.47(1)$ [Zn] were determined from XRD and EPMA results. Rietveld refinement of combined XRD/neutron powder diffraction data was carried out on undoped $La_4BaCu_5O_{13+\delta}$ and $x = 1$ for M = Fe, Co, Ni. For $La_4BaCu_5O_{13+\delta}$, which is an oxygen-deficient perovskite, the presence of square planar CuO_4 groups, disordered over the Cu(2) sites with CuO_5 square pyramids, is indicated, together with, for $\delta < 0$, either square planar CuO_4 or square pyramidal CuO_5 and octahedral CuO_6 groups disordered over the Cu(1) sites. For M = Fe, Ni, there was preferential substitution onto the one-fold octahedral site; for M = Co, substitution took place on both the one-fold octahedral and four-fold square pyramidal sites.
© 2002 Elsevier Science (USA). All rights reserved.

1. Introduction

The oxygen-deficient perovskite $La_4BaCu_5O_{13+\delta}$, first reported by Michel et al., is tetragonal, space group $P4/m$, $a \approx \sqrt{5}a_p = 8.644$ Å, $c \approx a_p = 3.867$ Å, where a_p refers to a perovskite subcell [1]. The structure, Fig. 1, has groups of four corner-sharing CuO_5 pyramids linked through CuO_6 octahedra [2]. Each octahedron shares four corners with four pyramids and two corners with two other octahedra; each pyramid is connected to four other pyramids and one octahedron [2]. The framework exhibits one perovskite-like tunnel and two hexagonal tunnels per cell [2]. Ba^{2+} and La^{3+} are ordered, with 12-coordinate Ba^{2+} in perovskite tunnels and 10-coordinate La^{3+} in hexagonal tunnels [2, 3].

The oxygen content is sensitive to processing conditions and values range from 12.5 to 13.2 [1, 3, 4]. On heating $La_4BaCu_5O_{13+\delta}$ under reducing conditions (15% H_2/85% Ar), three metastable phases with $\delta = -0.5$, –1.0 and –2.0 were stabilized [3]. $La_4BaCu_5O_{11}$ is tetragonal, $P4/m$; $a = 8.884(1)$ Å, $c = 3.714(1)$ Å, $La_4BaCu_5O_{12}$ is monoclinic, $P2/m$; $a = 8.878(2)$ Å, $b = 3.776(2)$ Å, $c = 8.702(2)$ Å; $\beta = 91.41(3)°$, $La_4BaCu_5O_{12.5}$ is also monoclinic with somewhat different cell dimensions [3, 4]. On heating it transforms to tetragonal symmetry at 690°C [4] and above 690°C, compositions: $0 > \delta > -0.5$ form a tetragonal solid solution [4]. At lower temperatures, most compositions in this range form a mixture of monoclinic $La_4BaCu_5O_{12.5}$ and tetragonal $La_4BaCu_5O_{\sim 13.0}$ [3, 4].

In addition to the various monoclinic and tetragonal phases, all of which are related to the perovskite subcell by a $\sqrt{5} \times \sqrt{5} \times 1$ supercell, a $\sqrt{10} \times \sqrt{10} \times 1$ supercell has been reported for $\delta = -0.5$ [4] and $\delta = 0.16$ [2]; the structural origin of the supercell in the latter has been attributed to the ordering of excess oxygen [2, 7].

$La_4BaCu_{5-x}M_xO_{13+\delta}$: M = Ni, Co, $0 \le x \le 1$; Fe, $x \le 0.5$ were synthesized by low-temperature NaOH–KOH flux methods [6, 7]. It was claimed that use of fluxes was essential, as these compounds could not be synthesized by the solid-state route [6]. Rietveld refinement of neutron powder data for $x = 1.0$, M = Ni, Co, showed Ni^{3+} and Co^{3+} to partially occupy the one-fold octahedral and four-fold square pyramidal sites [7]. Increased oxygen content was observed with Ni- and Co-substitution, leading to an increase in unit-cell volume [7]. The undoped and Ni-doped phases are metallic, Pauli paramagnets; the Co- and Fe-doped materials show a metal-to-insulator transition with increasing x and are weakly paramagnetic [1, 6].

In this study, we have investigated $La_4BaCu_5O_{13+\delta}$ by Rietveld refinement, obtained solid solution limits for $La_4BaCu_{5-x}M_xO_{13+\delta}$ (M = Ni, Co, Fe, Zn) for samples prepared by the solid-state route, and refined the

0022-4596/03/$ - see front matter © 2002 Elsevier Science (USA). All rights reserved.
PII: S0022-4596(02)00019-1

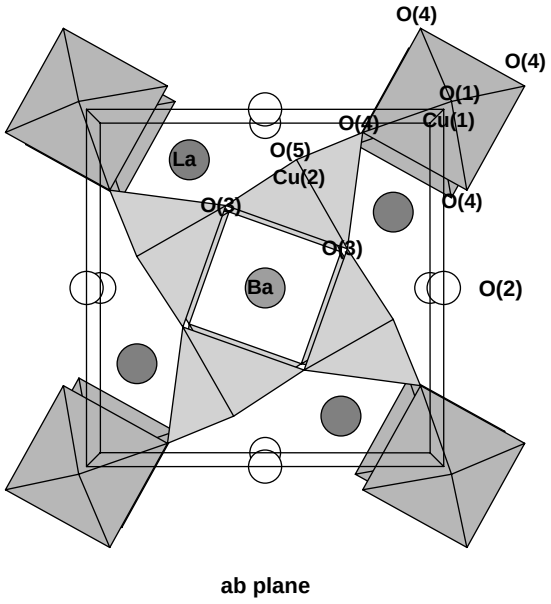

Fig. 1. Structure of $La_4BaCu_5O_{13}$; open circles represent vacant oxygen sites, O(2).

structures of $x = 1.0$, M = Ni, Co, Fe. Unsuccessful attempts were made to introduce Al, Mg, Cr and Mn into the $La_4BaCu_5O_{13+\delta}$ structure.

2. Experimental

Materials were prepared from stoichiometric amounts of dried, high-purity La_2O_3, $BaCO_3$, CuO, NiO, Co_3O_4, Fe_2O_3, MnO_2, ZnO, Al_2O_3 and Cr_2O_3. Powders were ground in an agate mortar and fired at 1000°C. Co- and Fe-substituted samples were additionally ball-milled, using Fritsch Pulverisette equipment, for 5 min at 500 rpm prior to firing.

High-resolution powder XRD data were collected on a Stoe STADI-P diffractometer in transmission mode, with a small linear position sensitive detector (PSD), Ge monochromator and Co$K\alpha_1$ radiation. Data were collected over the $20° \leq 2\Theta \leq 130°$ range, stepwidth 0.1°, count time 45 s. Patterns were indexed using Stoe software packages. Neutron powder diffraction data were collected on the POLARIS diffractometer, at the UK spallation source ISIS (Rutherford Appleton Laboratory), from the highest resolution backscattering detectors ($2\Theta = 145°$), over a time-of-flight range of 2000–19,500 μs. Structural characterization used the GSAS Rietveld program on XRD, neutron and combined XRD/neutron powder diffraction data. Results presented here used combined neutron and XRD data, although no significant differences were found when neutron data alone were refined.

Phase compositions were obtained by electron probe microanalysis (EPMA) using Cameca SX51 apparatus. Thermogravimetry, TG was used to calculate oxygen contents, by heating samples under a stream of 5%H_2/N_2 gas. Variation in oxygen content with temperature was measured by TG, using Stanton Redcroft STA1500 simultaneous TG-DTA equipment.

3. Results and Discussion

3.1. $La_4BaCu_5O_{13+\delta}$

XRD and EPMA results indicated that $La_4BaCu_5O_{13+\delta}$ was phase-pure after solid-state reaction at 1000°C for 7 nights; long reaction times were required to obtain a homogeneous single-phase material, as determined by EPMA. The XRD pattern was indexed on tetragonal symmetry, Table 1. From quantitative EPMA data, the scaled formula $La_{4.03(2)}Ba_{0.97(1)}Cu_{4.91(2)}O_{13+\delta}$ was determined; the slightly low Cu content was thought due to either Cu volatilization at high temperatures or the quality of Cu standard used for calibration rather than to a genuine non-stoichiometry (we have encountered similar effects with other cuprates).

Samples were post-reaction heat-treated by either slow-cooling or quenching from 1000°C; from H_2-reduction TG data, the oxygen contents were $-0.3(1) \leq \delta \leq 0.2(1)$, similar to that reported by TG in air up to 1015°C [3]. In order to try and increase the oxygen content, samples were heated at 500°C under O_2 at 1 atm and also slowly cooled from 700°C under 50 atm O_2, but these did not lead to an oxygen content value higher than 13.2.

Variation in oxygen content with temperature was measured by TG, Fig. 2. Initial oxygen content, $O_{12.85}$, of a sample prepared by normal cooling in air from 1000°C, decreased to $O_{12.64}$ under O_2 at 1000°C, and to $O_{12.49}$ in air at 1000°C; oxygen loss was completely reversible on cooling. Under N_2, oxygen content decreased to $O_{12.31}$ by 920°C at which temperature decomposition commenced. The observed loss of 0.36 oxide ions on heating to 1000°C in flowing air, Fig. 2, is similar to the value 0.43 reported on heating to 1015°C [3]. Results are also approximately consistent with the range $O_{12.5}$ to $O_{13.0}$ based on TG results in air [4]. There is general agreement, therefore, that the oxygen content in non-reducing atmospheres can vary by ~0.5–0.7

Table 1
Lattice parameters of tetragonal $La_4BaCu_4MO_{13+\delta}$, space group $P4/m$

	$La_4BaCu_5O_{12.9(1)}$	$La_4BaCu_4NiO_{13.0(1)}$	$La_4BaCu_4CoO_{12.98(5)}$	$La_4BaCu_4FeO_{12.9(1)}$
a (Å)	8.6456(3)	8.6170(2)	8.6094(4)	8.6357(3)
c (Å)	3.8594(2)	3.8778(2)	3.8861(4)	3.9071(3)
V (Å^3)	288.48(1)	287.94(1)	288.04(2)	291.37(2)

oxygens; there is some uncertainty over the exact range, although all studies agree that this includes the 'stoichiometric' composition $La_4BaCu_5O_{13}$.

Using the structure reported in [2] as a starting model, Rietveld refinement of combined XRD/neutron data for $La_4BaCu_5O_{12.9(1)}$, gave results in fair agreement with those reported for $\delta = 0.16$ (2), but with some vacancies in the O(1) site (apices of the $Cu(1)O_6$ octahedra) and with the O(2) site empty, Table 2. The higher oxygen content in [2] is the probable source of the slightly different results. The oxygen content calculated here from refined oxygen occupancies, 12.93(1), is in excellent agreement with that calculated from TG data, 12.9(1).

At this stage, the bond lengths were close to those reported [2]. The $Cu(2)O_5$ square pyramids, with four average Cu–O distances and one longer distance, show Jahn-Teller distortion attributed to unequal occupancy of d_{z^2} and $d_{x^2-y^2}$ orbitals, characteristic of Cu^{2+} (d^9) ions. The average Cu oxidation state is calculated to be ~2.4, suggesting three Cu^{2+} and two Cu^{3+} per unit cell. Cu^{3+} usually favors octahedral or square planar coordination and was expected to be present in the one-fold $Cu(1)O_6$ octahedra; these are compressed along the c-axis, with Cu(1)–O(1) bonds, 1.92905(1) Å, shorter than Cu(1)–O(4) bonds, 2.0322(8) Å. However, to maintain the average Cu oxidation state of 2.4+, Cu^{3+} must also be present on the square pyramidal sites, which cannot be occupied exclusively by Cu^{2+}. (Note: It is an idealized scheme to write the Cu species as purely ionic Cu^{2+}, Cu^{3+}, etc. since there is considerable charge delocalization associated with the high conductivity; a similar situation exists with other cuprates, such as $YBa_2Cu_3O_7$).

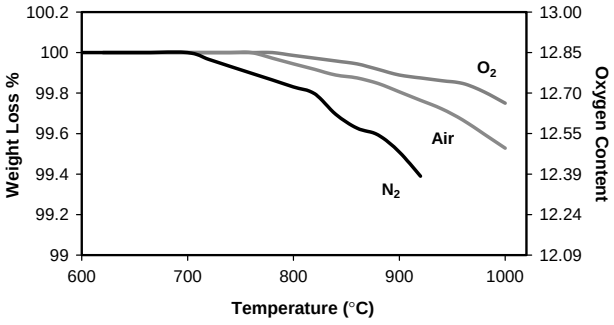

Fig. 2. Variation of oxygen content in $La_4BaCu_5O_{12.85}$ under different atmospheres.

From Table 2, U_{iso} for Cu(2) is larger than that for Cu(1), which may indicate that Cu(2) is displaced slightly off the site, or is split into two sites. The effect of splitting into two sites, Cu(2a) and Cu(2b), with fixed U_{iso}'s of 0.002, equal to that of Cu(1) was investigated. Occupancies were fixed at 0.25 and 0.75, respectively, consistent with an expected distribution of one Cu^{3+} and three Cu^{2+}. The refined position of Cu(2a) is considerably different from that of Cu(2), with significant displacement of the y coordinate towards the basal oxygen positions of the square pyramidal site, whereas Cu(2b) was displaced in the opposite direction towards the apical oxygen. As a final step, the positions and U_{iso} values were refined simultaneously; results are also given in Table 2. Since Cu(2a) is displaced towards the base of the square pyramid, the apical Cu(2a)–O3 bond is now much longer than the other four bonds and the coordination may be regarded as square planar, whereas Cu(2b) still retains square pyramidal coordination, albeit with a long Cu(2b)–O3 bond, Table 3.

These results indicate that the $Cu(2)O_5$ square pyramids obtained from the initial refinement may

Table 2
Refined atomic coordinates and U_{iso}'s of $La_4BaCu_5O_{12.9(1)}$, and refined atomic positions of Cu(2a) and Cu(2b)

Atom	x	y	z	Occ.	U_{iso} (Å^2)	Wyckoff
$La_4BaCu_5O_{12.9(1)}$						
Ba	0.5	0.5	0.5	1	0.0094(3)	1*d*
La	0.12685(5)	0.27768(6)	0.5	1	0.00499(6)	4*k*
Cu(1)	0	0	0	1	0.0020(2)	1*a*
Cu(2)	0.41491(6)	0.17195(6)	0	1	0.00444(7)	4*j*
O(1)	0	0	0.5	0.93(1)	0.0045(4)	1*b*
O(2)	0	0.5	0	0	—	2*e*
O(3)	0.26836(9)	0.39234(8)	0	1	0.0074(1)	4*j*
O(4)	0.22622(9)	0.06376(9)	0	1	0.0071(1)	4*j*
O(5)	0.4156(1)	0.15656(9)	0.5	1	0.0098(1)	4*k*
wRp = 0.0239 [ND]		wRp = 0.0480 [XRD]			wRp = 0.0286 [Total]	
Rp = 0.0379 [ND]		Rp = 0.0348 [XRD]			Rp = 0.0348 [Total]	
Chi^2 = 2.941		a = 8.64647(3) Å			c = 3.85810(2) Å	
Cu(2a) and Cu(2b)						
Cu(2a)	0.4191(3)	0.1588(3)	0	0.25	0.0019(5)	4*j*
Cu(2b)	0.4137(1)	0.1760(1)	0	0.75	0.0036(2)	4*j*

represent an average, in an approximate 1:3 ratio, of a $Cu(2a)O_4$ square plane, containing Cu^{3+} and three $Cu(2b)O_5$ square pyramids, containing Cu^{2+}, per unit cell. A final profile fit to the neutron data is shown in Fig. 3.

Bond valence sum calculations [8] were used to seek information on the Cu oxidation states in Cu(1) and Cu(2) sites; results are summarized in Table 3; calculations were performed assuming the two sites were occupied by either Cu^{2+} or Cu^{3+} and also for the Cu(2) site split into Cu(2a) and Cu(2b). Results demonstrate that the Cu(1) site is preferentially occupied by Cu^{3+} whereas the Cu(2) site, split or unsplit, is occupied by a $Cu^{2+,3+}$ mixture; the calculations are insufficiently sensitive to discriminate between Cu(2a) and Cu(2b) sites.

Table 3
Selected bond lengths of $La_4BaCu_5O_{12.9(1)}$ and bond valence sum calculations

M–O	Distance (Å)	*M*–O	Distance (Å)
La–O1	2.6396(5) [×0.93]	Cu1–O1	1.92905(1) [×1.86]
La–O3	2.4902(5) [×2]	Cu1–O4	2.0322(8) [×4]
La–O4	2.8072(6) [×2]	Cu2a–O3	2.425(2) [×1]
La–O4′	2.5760(6) [×2]	Cu2a–O3′	1.897(3) [×1]
La–O5	2.725(1) [×1]	Cu2a–O4	1.850(3) [×1]
La–O5′	2.7076(9) [×1]	Cu2a–O5	1.92931(4) [×2]
La–O5″	2.6642(9) [×1]	Cu2b–O3	2.2519(6) [×1]
Ba–O3	2.9324(5) [×8]	Cu2b–O3′	1.856(1) [×1]
Ba–O5	3.0578(8) [×4]	Cu2b–O4	1.891(1) [×1]
		Cu2b–O5	1.93661(6) [×2]

Site	$V(ro_{Cu^{2+}})1$[a]	$V(ro_{Cu^{3+}})1$[b]
Cu(1)	2.36	3.01
Cu(2)	2.20	2.80
Cu(2a)	2.18	2.75
Cu(2b)	2.21	2.81

[a] $ro_{Cu^{2+}} = 1.649$.
[b] $ro_{Cu^{3+}} = 1.739$.

We may now speculate on the consequences of varying oxygen content. For $\delta = 0$, the O(1) site is full and the Cu(1) octahedra, consisting of four O(4) and two O(1), are complete and contain Cu^{3+} exclusively. The Cu(2) site contains a mixture of square planar Cu^{3+} (but with a very long bond to a fifth oxygen) and square pyramidal Cu^{2+}, in the ratio 1:3.

For $\delta > 0$, partial occupancy of the O(2) sites occurs, thus converting some Cu(2) polyhedra to octahedra together with an increase in the Cu^{3+} content in the Cu(2) sites. Each added O(2) links two $Cu(2)O_6$ octahedra, consistent with oxidation of two adjacent Cu^{2+} ions to Cu^{3+} ions. The $\sqrt{10}a_p \times \sqrt{10}a_p \times a_p$ supercell reported for $La_4BaCu_5O_{13.16}$ [2] was attributed to distortion in the $[Cu_5O_{13}]$ matrix, induced by the introduction of oxygen into half of the hexagonal tunnels [2]. However, the possibility that this supercell is caused by ordering of Cu^{3+} and Cu^{2+} within the Cu(2) sites needs to be considered.

Structural studies on oxygen-rich compositions [2], which showed partial occupancy of the O(2) sites, gave extremely short Cu(2)–O(2) distances, ~1.65–1.71 Å, for which we can offer an explanation in terms of splitting of the Cu(2) sites; the Cu(2a)–O(2) distance is impossibly short, ~1.52 Å and therefore, adjacent Cu(2a) and O(2) sites are unlikely to be occupied simultaneously. The Cu(2b)–O(2) distance is longer, 1.70 Å and closer to an acceptable value. Our model assumes a splitting into two positions for Cu(2); in reality, there may be a distribution of positions, dependent on whether or not adjacent O(2) positions are occupied. Thus, the Cu(2) position splits, even in the absence of any O(2) oxygens and reflects the presence of

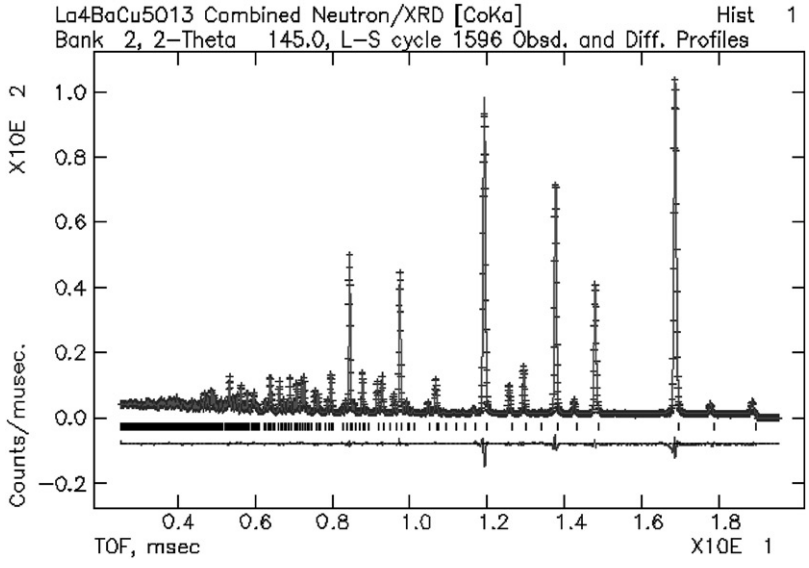

Fig. 3. Observed, Difference and Calculated Neutron Profiles for $La_4BaCu_5O_{12.9(1)}$.

both Cu^{2+} and Cu^{3+} ions. With some O(2) sites occupied, additional displacement of Cu(2b) positions may occur, increasing the Cu(2b)–O(2) distance still further and at the same time, reducing the Cu(2b)–O(3) distance. This displacement of Cu(2b) converts the site coordination into a more regular octahedral site with comparable Cu–O bond lengths, consistent with occupancy by Cu^{3+} ions.

For $\delta<0$, the O(1) site is increasingly depopulated, thereby reducing the number of $Cu(1)O_6$ octahedra; these sites become increasingly square pyramidal (or square planar, depending on the distribution of oxygen vacancies), consistent with an increase in Cu^{2+} content in these sites. The structure is, however, likely to be complex for all oxygen contents (other than 13.0), since both Cu(1) and Cu(2) sites consist of polyhedral averages and both can contain Cu^{2+} and Cu^{3+} ions which could, in principle, be either ordered or disordered! The model proposed here, with vacancies on the O(1) sites of the $Cu(1)O_6$ octahedra is different to that proposed in [3] in which the oxygen vacancies occur in the equatorial O(4) sites leaving O(1) fully occupied to form linear, two-coordinate Cu(1) containing Cu^{+} in the fully reduced phase $La_4BaCu_5O_{11}$. However, our model, with O(1) vacancies, is consistent with the structure of $La_4BaCu_5O_{12}$ [7] in which O(1) sites are empty, giving, effectively, $Cu(1)O_4$ square planar units in the *ab* plane, which link rings of $Cu(2)O_5$ square pyramids in the same way that the $Cu(1)O_6$ octahedra link the pyramids in $La_4BaCu_5O_{13+\delta}$.

3.2. $La_4BaCu_{5-x}M_xO_{13+\delta}$: M=Ni, Co, Fe

$La_4BaCu_{5-x}M_xO_{13+\delta}$: M = Ni, Co, Fe is structurally analogous to $La_4BaCu_5O_{13}$, Fig. 1, with a framework of $(Cu/M)O_x$ polyhedra and similar distribution of La, Ba and vacancies [4, 6]. For M = Ni, our EPMA results on fully reacted samples gave a solid solution limit of $x = 1.56(7)$. Again, long reaction times were required to produce single-phase, homogeneous materials. For M = Co and Fe, ball-milling of powders, in addition to long reaction times, was required to produce single-phase materials; solid solution limits of $x = 1.1(1)$ and 1.0(1), respectively, were determined from EPMA. Lattice parameters for $La_4BaCu_4NiO_{13.0(1)}$, $La_4BaCu_4CoO_{12.98(5)}$ and $La_4BaCu_4FeO_{12.9(1)}$ are shown in Table 1. Oxygen contents were calculated from H_2-reduction TG data.

Rietveld refinement was carried out for $x = 1.0$, M = Ni, Co, Fe. Initially, it was assumed that Cu and M were ordered over the four-fold square pyramidal and one-fold octahedral sites in a 4:1 ratio. However, refinement of neutron data showed large differences between U_{iso}'s for Cu(2) and M(1); site occupancies were therefore varied, whilst retaining the overall 4:1 ratio of Cu:M. Graphs of refined U_{iso} values against site occupancies, expressed as the percentage of Ni, Co and Fe on the Cu(1) site, are shown in Figs. 4–6.

To interpret these results, we assume that the most probable structure has two Cu sites with similar U_{iso} values. This, of course, ignores the possibility of site splitting and consequent modification of the U_{iso} value of the Cu(2) site, as found for $La_4BaCu_5O_{13+\delta}$. With this assumption, Fig. 4 indicates that $La_4BaCu_4NiO_{13.0(1)}$ is fully ordered, with Ni on octahedral Ni(1) sites and Cu on square pyramidal Cu(2) sites. At

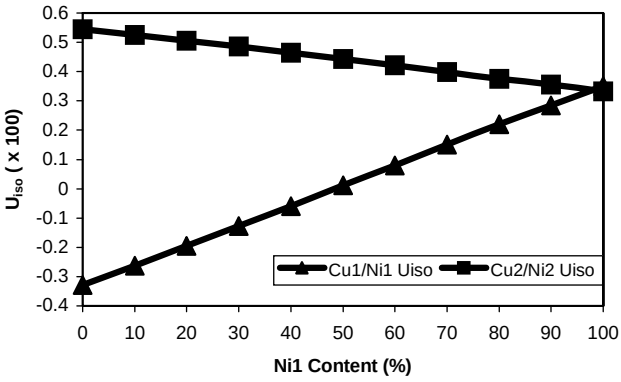

Fig. 4. Plot of Ni1 content versus U_{iso}.

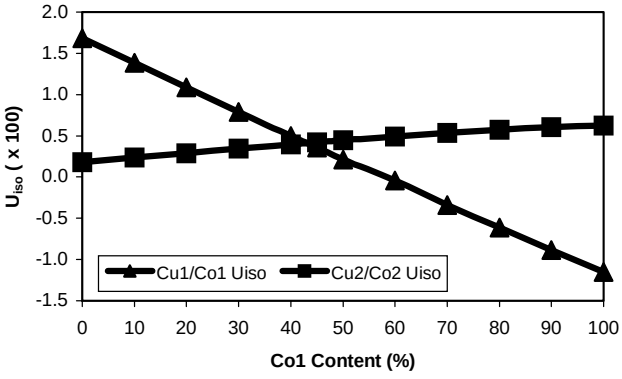

Fig. 5. Plot of Co1 content versus U_{iso}.

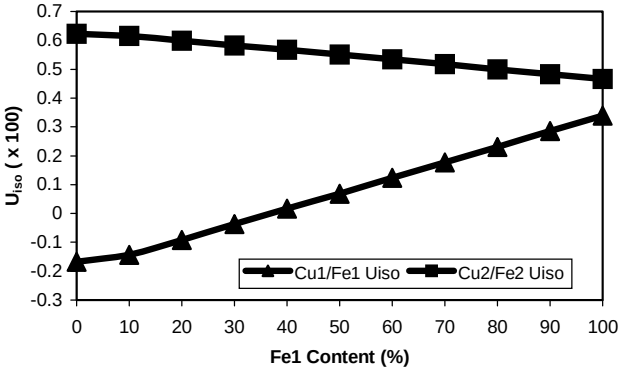

Fig. 6. Plot of Fe1 content versus U_{iso}.

present, we have no information on the oxidation states of Ni and Cu, i.e., whether they are $Ni^{2+}Cu_2^{2+}Cu_2^{3+}$ or $Ni^{3+}Cu_3^{2+}Cu^{3+}$ or some other combination. Similarly, Fe(1) and Cu(2) are fully ordered over octahedral and square pyramidal sites in $La_4BaCu_4FeO_{12.9(1)}$.

For Co, the U_{iso} values indicate equal distribution of Cu, Co over the octahedral site, with Cu predominantly, but not exclusively, in the square pyramidal sites. The occupancies indicated in Figs. 4–6 were used in the final refinements, Tables 4–6, with bond lengths in Tables 7–9.

The results are very similar to those obtained for $La_4BaCu_5O_{13+\delta}$. Bond lengths and polyhedral dimensions are comparable; the long Cu(2)–O3 (M = Ni, Fe), and Cu/Co(2)–O3 (M = Co) bonds are characteristic of Jahn–Teller distortion indicating the possible presence of Cu^{2+} (Cu^{2+}/Co^{2+}) on the square pyramidal sites. However, lattice parameters showed an a-axis contraction and c-axis expansion on substitution leading to elongation of bonds along the c-axis, and contraction of certain bonds in the ab plane.

In the parent material, Cu^{3+} occupies the one-fold octahedral site; it is known that Ni^{3+}, Co^{3+} and Fe^{3+} favor octahedral coordination [4]. From the results presented here, Ni and Fe appear to substitute preferentially and Co partially onto the octahedral site. The octahedral radii of Cu^{3+} (0.68 Å), Ni^{3+} (0.70 Å), Fe^{3+} (0.69 Å) and Co^{3+}(0.68 Å) are very similar; consequently, from purely size considerations, these ions could readily substitute for octahedral Cu^{3+}.

As a final stage, the Cu(2) site was split into 2(a) and 2(b) sites. For M = Ni, the Cu(2a) and 2(b) positions were displaced significantly from the average Cu(2) position, Table 4, Fig. 7, similar to $La_4BaCu_5O_{13+\delta}$. For M = Fe, the displacements were much less (not shown) and therefore, this site was not split in the final refinement, Table 5. For M = Co, such splitting was not investigated since the Cu(2) site contains a mixture of

Table 4
Refined atomic positions and U_{iso}'s for $La_4BaCu_4NiO_{13.0(1)}$ and Cu(2a) and Cu(2b)

Atom	x	y	z	Occ.	U_{iso} (Å^2)	Wyckoff
$La_4BaCu_4NiO_{13.0(1)}$						
Ba	0.5	0.5	0.5	1	0.0081(2)	1*d*
La	0.12506(6)	0.27908(6)	0.5	1	0.0046(1)	4*k*
Ni(1)	0	0	0	1	0.0035(1)	1*a*
Cu(2)	0.41198(6)	0.17418(6)	0	1	0.0034(1)	4*j*
O(1)	0	0	0.5	0.95(1)	0.0039(3)	1*b*
O(2)	0	0.5	0	0	—	2*e*
O(3)	0.26832(9)	0.39254(9)	0	1	0.0070(1)	4*j*
O(4)	0.2214(1)	0.06260(9)	0	1	0.0060(1)	4*j*
O(5)	0.4140(1)	0.1570(1)	0.5	1	0.0093(1)	4*k*
wRp = 0.0246 [ND]		wRp = 0.0387 [XRD]			wRp = 0.0286 [Total]	
Rp = 0.0415 [ND]		Rp = 0.0287 [XRD]			Rp = 0.0288 [Total]	
Chi^2 = 1.907		a = 8.61659(2) Å			c = 3.87694(2) Å	
Cu(2a) and Cu(2b)						
2a	0.4177(3)	0.1593(2)	0	0.25	0.0004(3)	4*j*
2b	0.4104(1)	0.17848(8)	0	0.75	0.0022(1)	4*j*

Table 5
Refined atomic positions and U_{iso}'s of $La_4BaCu_4FeO_{12.9(1)}$

Atom	x	y	z	Occ.	U_{iso} (Å^2)	Wyckoff
Ba	0.5	0.5	0.5	1	0.0082(4)	1*d*
La	0.1229(1)	0.2841(1)	0.5	1	0.0067(1)	4*k*
Fe(1)	0	0	0	1	0.0033(2)	1*a*
Cu(2)	0.4151(1)	0.1715(1)	0	1	0.0044(1)	4*j*
O(1)	0	0	0.5	0.96(1)	0.0038(4)	1*b*
O(2)	0	0.5	0	0	—	2*e*
O(3)	0.2677(2)	0.3912(2)	0	1	0.0097(2)	4*j*
O(4)	0.2228(2)	0.0582(1)	0	1	0.0054(2)	4*j*
O(5)	0.4122(2)	0.1584(2)	0.5	1	0.0111(2)	4*k*
wRp = 0.0432 [ND]		wRp = 0.0487 [XRD]			wRp = 0.0450 [Total]	
Rp = 0.0691 [ND]		Rp = 0.0323 [XRD]			Rp = 0.0326 [Total]	
Chi^2 = 4.315		a = 8.63853(5) Å			c = 3.90398(3) Å	

Table 6
Refined atomic positions and U_{iso}'s of $La_4BaCu_4CoO_{12.98(5)}$

Atom	x	y	z	Occ.	U_{iso} (Å^2)	Wyckoff
Ba	0.5	0.5	0.5	1	0.0077(4)	1*d*
La	0.12272(7)	0.28007(8)	0.5	1	0.0061(1)	4*k*
Cu(1)	0	0	0	0.55	0.0038(3)	1*a*
Co(1)	0	0	0	0.45	0.0038(3)	1*a*
Cu(2)	0.41502(6)	0.17142(6)	0	0.8625	0.0040(1)	4*j*
Co(2)	0.41502(6)	0.17142(6)	0	0.1375	0.0040(1)	4*j*
O(1)	0	0	0.5	0.90(1)	0.0040(5)	1*b*
O(2)	0	0.5	0	0	—	2*e*
O(3)	0.2672(1)	0.3919(1)	0	1	0.0090(2)	4*j*
O(4)	0.2198(1)	0.0603(1)	0	1	0.0061(1)	4*j*
O(5)	0.4120(1)	0.1579(1)	0.5	1	0.0099(2)	4*k*
w*R*p = 0.0310 [ND]		w*R*p = 0.0495 [XRD]			w*R*p = 0.0365 [Total]	
*R*p = 0.0527 [ND]		*R*p = 0.0349 [XRD]			*R*p = 0.0351 [Total]	
Chi^2 = 2.752		*a* = 8.60946(4) Å			*c* = 3.88304(3) Å	

Table 7
Selected bond lengths of $La_4BaCu_4NiO_{13.0(1)}$

M–O		*M*–O	Distance (Å)
La–O1	2.6351(6) [× 0.95]	Ni1–O1	1.93847(1) [× 1.90]
La–O3	2.4975(6) [× 2]	Ni1–O4	1.9826(9) [× 4]
La–O4	2.8154(7) [× 2]	Cu2a–O3	2.387(2) [× 1]
La–O4′	2.5728(6) [× 2]	Cu2a–O3′	1.886(3) [× 1]
La–O5	2.703(1) [× 1]	Cu2a–O4	1.886(3) [× 1]
La–O5′	2.695(1) [× 1]	Cu2a–O5	1.93882(5) [× 2]
La–O5″	2.659(1) [× 1]	Cu2b–03	2.2137(6) [× 1]
Ba–O3	2.9326(5) [× 8]	Cu2b–03	1.866(1) [× 1]
Ba–O5	3.0466(9) [× 4]	Cu2b–04	1.910(1) [× 1]
		Cu2b–05	1.94750(6) [× 2]

Table 8
Selected bond lengths of $La_4BaCu_4FeO_{12.9(1)}$

M–O	Distance (Å)	*M*–O	Distance (Å)
La–O1	2.674(1) [× 0.96]	Fe1–O1	1.95199(2) [× 1.92]
La–O3	2.496(1) [× 2]	Fe1–O4	1.990(2) [× 4]
La–O4	2.892(1) [× 2]	Cu2–O3	2.2853(15) [× 1]
La–O4′	2.5572(9) [× 2]	Cu2–O3	1.8688(18) [× 1]
La–O5	2.725(2) [× 1]	Cu2–O4	1.9274(18) [× 1]
La–O5′	2.670(2) [× 1]	Cu2–O5	1.95543(11) [× 2]
La–O5″	2.641(2) [× 1]		
Ba–O3	2.9532(9) [× 8]		
Ba–O5	3.047(2) [× 4]		

Table 9
Selected bond lengths of $La_4BaCu_4CoO_{12.98(5)}$

M–O	Distance (Å)	*M*–O	Distance (Å)
La–O1	2.6326(8) [× 0.90]	Ba–O3	2.9420(7) [× 8]
La–O3	2.4984(8) [× 2]	Ba–O5	3.042(1) [× 4]
La–O4	2.8370(8) [× 2]	Cu/Co(1)–O1	1.94152(1) [× 1.80]
La–O4′	2.5537(7) [× 2]	Cu/Co(1)–O4	1.962(1) [× 4]
La–O5	2.703(1) [× 1]	Cu/Co(2)–O3	2.285(1) [× 1]
La–O5′	2.669(1) [× 1]	Cu/Co(2)–O3′	1.856(1) [× 1]
La–O5″	2.669(1) [× 1]	Cu/Co(2)–O4	1.934(1) [× 1]
		Cu/Co(2)–O5	1.94521(8) [× 2]

Cu and Co and the number of parameters was too great to make any refinement meaningful, Table 6.

In the literature, from neutron diffraction data of $La_4BaCu_4NiO_{13.20}$ and $La_4BaCu_4CoO_{13.35}$, prepared by the low-temperature flux method, it was suggested that Ni and Co would be present as trivalent cations, due to the highly oxidizing nature of the synthesis [6, 7] and consistent with their higher oxygen content compared with those prepared here. Ni^{3+} was present in both one-fold octahedral and four-fold square pyramidal sites, in a Cu(1) to Ni(1) ratio of 0.66:0.34 [7]. This is different from the results found here and could reflect a change in the location of the Ni on oxidation. Co^{3+} also occupied both the one-fold octahedral and four-fold square pyramidal sites, with a Cu(1) to Co(1) ratio of 0.54:0.46 [7], similar to that found here. No data were reported for $La_4BaCu_4FeO_{13+\delta}$, as it could not be prepared by the low-temperature flux method; the reported solid solution limit was $x = 0.5$, in $La_4BaCu_{5-x}Fe_xO_{13+\delta}$ [5].

3.3. $La_4BaCu_{5-x}M_xO_{13+\delta}$ (M=Mn, Zn, Al, Cr)

Attempts were made to synthesize $La_4BaCu_4MO_{13+\delta}$ (M = Mn, Zn, Al, Cr) by solid-state reaction at 1000°C over 7 nights. No single-phase samples were obtained, indicating solid solution limits were $x < 1.0$. For M = Zn, the solid solution limit was $x = 0.47(1)$ from EPMA data. No EPMA data were collected for M = Al, Cr. For M = Mn, very fine-grained and inhomogeneous samples were formed, and it was not possible to ascertain the solid solution limit by EPMA.

4. Conclusions

$La_4BaCu_5O_{13+\delta}$ was prepared phase-pure by solid-state reaction at 1000°C for 7 days; long reaction times

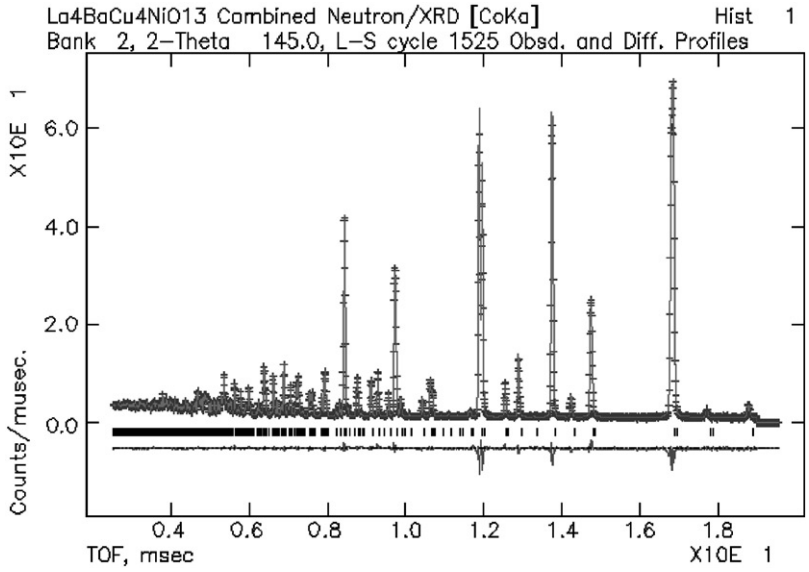

Fig. 7. Observed, Difference & Calculated Neutron Profiles for $La_4BaCu_4NiO_{13.0(1)}$.

were required to produce homogeneous single-phase material. Oxygen content was variable $-0.3(1) \leq \delta \leq 0.2(1)$ in reasonable agreement with literature. Variation of oxygen content with temperature was measured by TG. Oxygen loss up to 1000°C, under O_2 and air, was completely reversible on cooling; under N_2, decomposition occurred above 920°C. Rietveld refinement indicated the presence of CuO_4 square planes disordered with CuO_5 square pyramids on the Cu(2) sites. A model for the variation in crystal structure with oxygen content δ is presented. The structure is complex for all oxygen contents (other than 13.0), since both Cu(1) and Cu(2) sites consist of polyhedral averages and both can contain Cu^{2+} and Cu^{3+} ions which could, in principle, be either ordered or disordered.

$La_4BaCu_{5-x}M_xO_{13+\delta}$ (M = Ni, Co, Fe, Zn) was prepared by the solid-state route at 1000°C. Solid solution limits of $x = 1.56(7)$ [Ni], $x = 1.1(1)$ [Co], $x = 1.0(1)$ [Fe] and $x = 0.47(1)$ [Zn] were determined. Co- and Fe-materials required ball-milling, prior to final heat treatment in order to eliminate completely second phases. For $La_4BaCu_4MO_{13+\delta}$, M = Ni, Fe, there was preferential substitution of M onto the one-fold octahedral site, whereas for M = Co, substitution took place on both the one-fold octahedral and four-fold square pyramidal sites. No $La_4BaCu_{5-x}M_xO_{13+\delta}$ (M = Mn, Al) materials were prepared phase-pure.

Acknowledgments

P.S.A. thanks the EPSRC for a studentship.

References

[1] C. Michel, L. Er-Rakho, B. Raveau, Mater. Res. Bull. 20 (1985) 667–671.
[2] C. Michel, L. Er-Rakho, M. Hervieu, J. Pannetier, B. Raveau, J. Solid State Chem. 68 (1987) 143–152.
[3] P.K. Davies, C.M. Katzan, J. Solid State Chem. 88 (1990) 368–383.
[4] M. Kato, N. Kojima, K. Yoshimura, Y. Ueda, N. Nakayama, K. Kosuge, Z. Hiroi, Y. Bando, J. Solid State Chem. 103 (1993) 253–262.
[5] N. Ravgavittal, G.N. Subanna, T.N. Guru Row, C.N.R. Rao, J. Solid State Chem. 114 (1995) 95–101.
[6] C. Shivakumara, M.S. Hegde, K. Sooryanarayana, T.N. Guru Row, G.N. Subbanna, J. Mater. Chem. 8 (1998) 2695–2700.
[7] C. Shivakumara, M.S. Hegde, H. Rajagopal, A. Sequiera, Mater. Res. Bull. 35 (2000) 2063–2068.
[8] I.D. Brown, D. Altermatt, Acta Crystallogr. B 41 (1985) 244–247.